Evaluation of DC electric field measurement by the double probe system aboard the Geotail spacecraft

Y. Kasaba[a], H. Hayakawa[a], K. Ishisaka[b], T. Okada[b], A. Matsuoka[a], T. Mukai[a], and Y. Takei[c]

[a]*Institute of Space and Astronautical Science (ISAS), Japan Aerospace Exploration Agency (JAXA), Sagamihara, Kanagawa 229-8510, Japan.* [b]*Toyama Prefectural University, Kosugi, Toyama 939-0398, Japan.* [c]*University of Tokyo, Tokyo 113-0033, Japan.*

Abstract

We summarize the characteristics of the DC electric field measurement by the double probe system, EFD-P, aboard Geotail. The accuracy and correction factors for the gain (effective length) and off-set, which depends on ambient plasma conditions, are provided.

1. Introduction

Accurate measurement of electric field is an essential request for studies of macroscopic plasma convection, microscopic wave-particle interactions, violation of MHD approximation, etc. One of typical measurement techniques is 'Double Probe method', identical to that of a voltmeter: the potential difference between two top-hat probes [cf. *Pedersen et al.,* 1984]. Double Probe method can measure electric field passively and continuously in all plasma conditions. However, the probe measurement is subjected to the variable gain (effective length) of the probe antenna and the artificial offset of the measured values. These parameters depend on a) the disturbance from ambient plasma and b) the disturbance from the spacecraft body, and as a result, the accuracy of the measured electric field values is limited. In this paper, we showed the results of the characteristics of DC electric field measurement by EFD-P aboard Geotail [*Tsuruda et al.*, 1994], in order to evaluate the accuracy, gain, and offset controlled by ambient plasmas.

2. EFD-P: PANT and EFD aboard the Geotail spacecraft

Figure 1 shows the PANT element. PANT is a pair of top-hat antennas composed of a conductive sphere (105 mm in diameter) attached at the tip of a stainless steel wire (50m in length). Wire surface except the outer portion (1 m) is coated with Polyimide film for insulation, and its inner portion is covered by a copper-mesh sleeve. The surface of the spheres and outer portion 1 m of wire is covered by Aerodag for photoelectron yield stabilization. Because of this design, PANT can act in different manners for DC and AC fields. For DC electric field (< ~100 Hz), PANT is coupled with the surrounding plasma at its top (Sphere and Conductive part of the wire), with effective resistance of several 10 MΩ and the effective length of ~50 m (antenna length). For AC electric field, PANT acts as a dipole wire antenna of 100m-tip-to-tip length, and couples to the plasma with capacity (~100pF) and the effective dipole length approximately 50 m (half of the length). Its output signal is transferred to EFD (Electric Field Detector) for DC fields and PWI (Plasma Wave Instrument) for AC fields. The EFD data was used for the present analysis.

a)

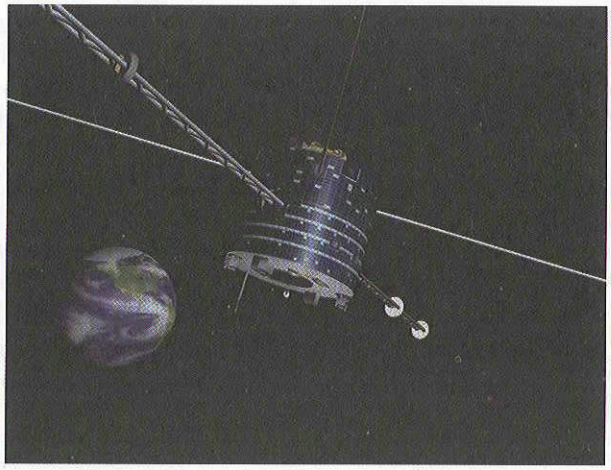

b)

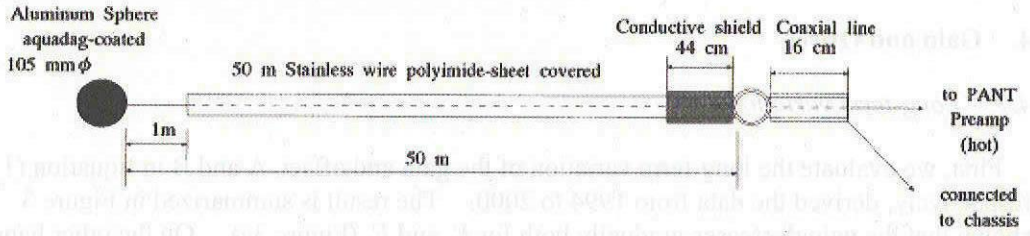

Figure 1. a) The Geotail spacecraft.
b) The PANT system aboard the Geotail spacecraft [*Tsuruda et al.*, 1994]

3. Data Sets

For the present analysis, the assumption $\boldsymbol{E} + \boldsymbol{v} \times \boldsymbol{B} = 0$ is used, where $\boldsymbol{E}$, $\boldsymbol{v}$, and $\boldsymbol{B}$ are electric field, plasma velocity, and magnetic field vectors, respectively. We compared DC electric field measured by EFD-P and $\boldsymbol{v} \times \boldsymbol{B}$ measured by LEP (Low Energy Plasma Analyzer) and MGF (Magnetic Field Experiment) aboard Geotail. The used data set is summarized in Table 1. The data are simultaneously obtained with 12 sec. time resolution. For the present analysis, the accuracy of $\boldsymbol{v}$ and $\boldsymbol{B}$ are essential.

Data selection criteria are shown in Table 2. The accurate analysis is limited before 1998 because the calibrated LEP data are unavailable after then yet. Even in 1993-1999, the particle data has errors because: 1) Limitation of ion measurement by LEP aboard Geotail: In high density region (i.e. magnetosheath & solar wind), LEP generally does not measure the energy range less than 40eV. It is for the request from the life of its sensor (MCP). Much counts cause damages. 2) Charge up of the spacecraft: In low density region (<< 0.1cc), the potential of the spacecraft is several 10s V. Low energy ion can not be observed in such case. 3) Limited field of view in Z-axis: LEP does not cover the region over ~75deg along spin axis. Conditions concerning to LEP in Table 2 are set for the rejection of those ambiguities. Electron data is less reliable by the contamination of photoelectrons, but the condition by the comparison between electrons and ions is effective to eliminate the bad data. Therefore, error becomes larger where the criteria are not adopted.

Figure 2 shows the relation between observed electric field by EFD-P, E_{obs} (Y-axis) and $-v_i \times B$ (X-axis) in 1994-1997, where v_i is ion velocity. At this analysis, we use the spacecraft coordinate, which difference to the GSE coordinate is several degrees. Majority of errors is from non-reliable v_i, caused by the limitation of energy range in high density region (lower limit: ~40 eV in usual), the lack of low energy part by spacecraft charge up in low density region, and limited field of view along Z-axis.

We assume $v_i \times B$ as real electric field, E_{real}. Observed electric field E_{obs} can be written as:

$$E_{obs}\ [\mathrm{mV/m}] = A \times E_{real} + B \qquad (1)$$

where A and B is gain (= 'effective length'/'actual antenna length') and offset, respectively. Table 3 shows the parameter A and B derived from Figure 2 fitted by the least mean square method. Gain A is ~0.7. Offset B is 0.4 mV/m for E_y and ~1.5 mV/m for E_x. Those tendencies are generally agreed with the ISEE results [Pedersen et al., 1984]. Since E_{real} has errors itself, the accuracy of E_{obs} is better than 0.6 mV/m for E_x and 0.3 mV/m for E_y, after the correction of gain and offset, respectively.

In Figure 2, there are still errors around $-v_i \times B \sim 0$, caused by the error in v_i, which was not rejected automatically by the current selection criteria. The refinement will be in the next work.

4. Gain and Offset

4.1. Long-term variation

First, we evaluate the long-term variation of the gain and offset, A and B in Equation (1), respectively, derived the data from 1994 to 2000. The result is summarized in Figure 3. It is shown that the gain decreases gradually both for E_x and E_y (Figure 3a). On the other hand, the offset is found to increase only for E_x, from ~1 mV/m to ~3 mV/m (Figure 3b). Both might be related to the enhancement of photoelectron non-uniformity around the spacecraft. Since the solar UV flux does not change significantly during 1994-1997, this could be caused by the increase of photoelectron production by the degradation of the spacecraft surface. On the other hand, degradation is not found in the accuracy of the electric field measurement (Figure 3c). It is noted that the difference between 1994 and 1995-2000 could be partly caused by the difference of orbit between 'Distant-tail phase' before Nov. 1994 and 'Near-tail phase' after that.

Instrument	Data	dT	Available data
LEP	Ion: density(N_i), velocity(v_i), temperature(T_i)	12 sec.	1993.9~
	Electron: density(N_e), velocity(v_e), temperature(T_e)	12 sec.	1993.9~1998.1
MGF	Magnetic field vector (B)	12 sec.	1992.9~
EFD-P	Electric field vector (E), Spacecraft potential (V_{sc})	12 sec.	1992.9~

Table 1. Data sets used in this analysis. For LEP, the data after 1998 is not calibrated.

Instrument	Condition	
LEP- electron	Reliable density & temperature	$N_i/N_e = 0.8\sim1.2$, $T_e > 20$eV
LEP- Ion	Reliable density & temperature	$Ni > 0.1\ N(V_{sc})$, $T_i > 20$eV
	EA mode	FOV: center of $\theta = +65.5^\circ \sim -65.5^\circ$
MGF	Stable B (in 12sec)	$B_{rms} < 0.05\ \|B\|$
EFD	Stable E (in 12sec)	$E_{rms} < 1.0$ mV/m
General	Normal potential	No eclipse, No potential control

Table 2. Data selection criteria. Criteria of 'LEP-electron' can only be applied to the data in 1994-1997. $N(V_{sc})$ is derived from plasma potential by Equation 5.

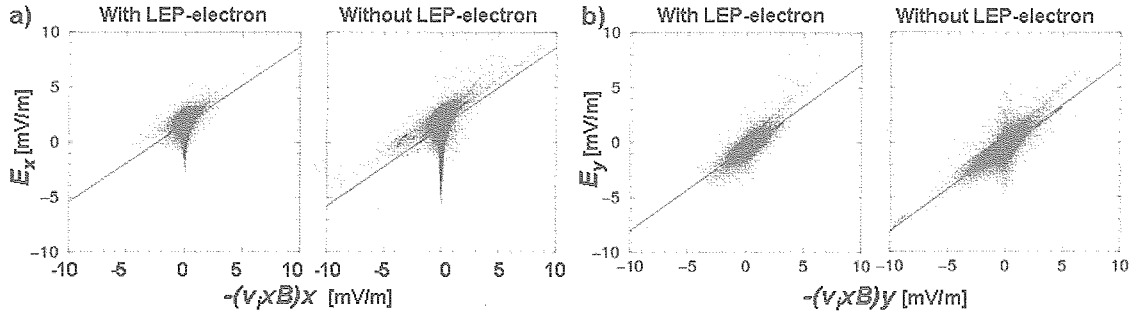

Figure 2. Relationship between E (Y-axis) and $-v_i \times B$ (X-axis) in 1993-1997: a) E_x and b) E_y. Line is the relation between them by the RMS fitting.

E_x	Criteria with LEP-electron	$(E_{obs})_x$ = +0.704 x $(E_{real})_x$ + 1.64	σ ~ 0.63 mV/m
	Criteria without LEP-electron	$(E_{obs})_x$ = +0.724 x $(E_{real})_x$ + 1.40	σ ~ 0.94 mV/m
E_y	Criteria with LEP-electron	$(E_{obs})_x$ = +0.756 x $(E_{real})_x$ - 0.44	σ ~ 0.33 mV/m
	Criteria without LEP-electron	$(E_{obs})_x$ = +0.768 x $(E_{real})_x$ - 0.38	σ ~ 0.46 mV/m

Table 3. Parameters fitted to '$E_{obs} = A \times E_{real} + B$' from Figure 2. A and B is gain and offset.

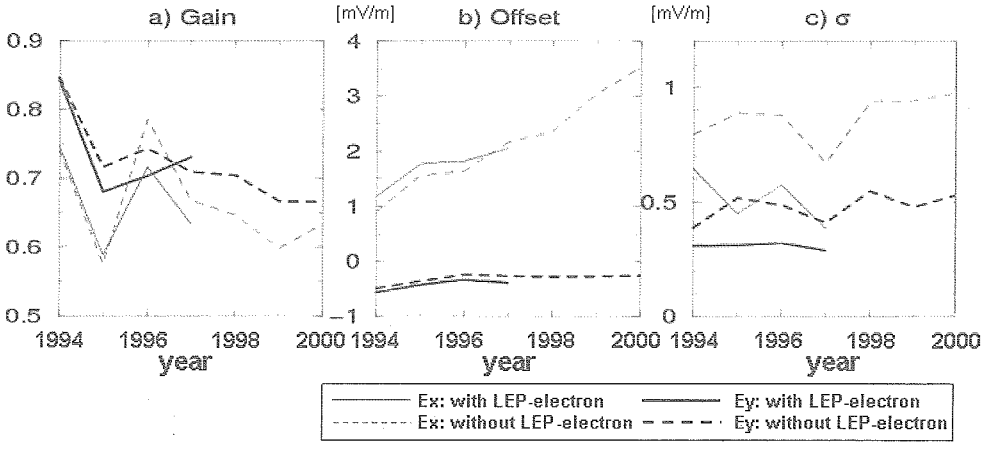

Figure 3. Time variation of a) Gain, b) Offset, and c) Error in 1994-2000.

4.2. *Correction by* V_{sc} and T_e (or T_i)

Here we try to refine significantly the correction formula, namely Equation (1), by taking into account the dependence of the fitting parameters (A and B) on the ambient plasma parameters. Since we can assume that the photoelectron outflow is constant due to the almost constant solar UV flux, the spacecraft potential is mainly determined by the inflow electron flux, which is proportional to $N_e v_e = N_e \sqrt{T_e}$. And photoelectron from and the potential structure around the spacecraft are as disturbance factors, which are related to the spacecraft potential V_{sc} and Debye length λ_D. Since λ_D and V_{sc} are controlled by N_e and T_e, independent parameters are two. In this analysis, we used V_{sc} and T_e as correction variables. Since the electron moment data is not always reliable, we also used ion temperature T_i. The accuracy in this case is worse because T_i is not always correlated to

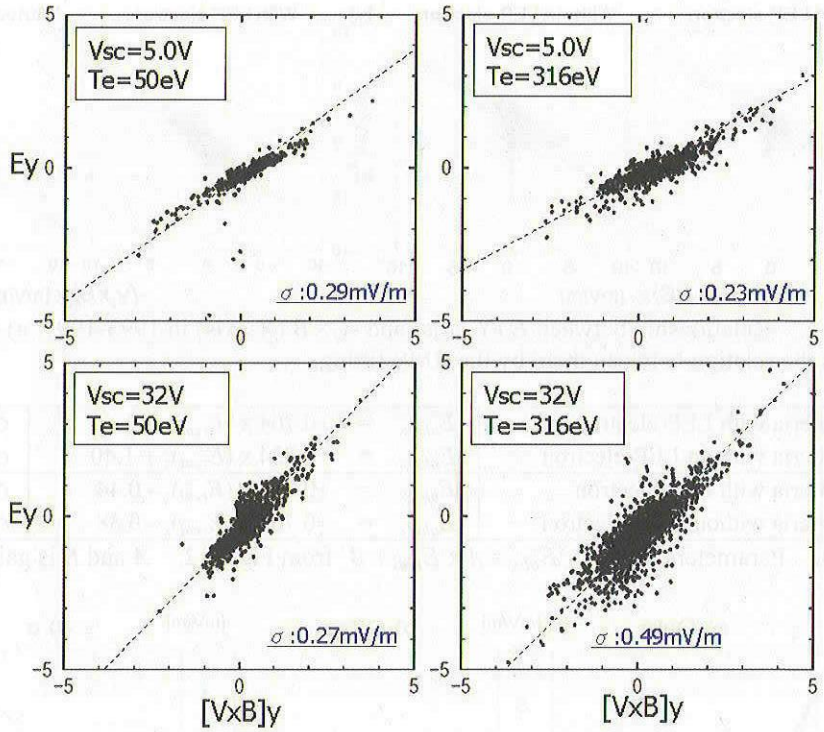

Figure 4. Relationship between $\boldsymbol{E}$ (Y-axis) and $-\boldsymbol{v}_i \times \boldsymbol{B}$ (X-axis) in 1993-1997, categorized by specific 'V_{sc}' (Upper: 5.0V, Lower: 32V) and 'T_e' (Left: 50eV, Right: 316eV).

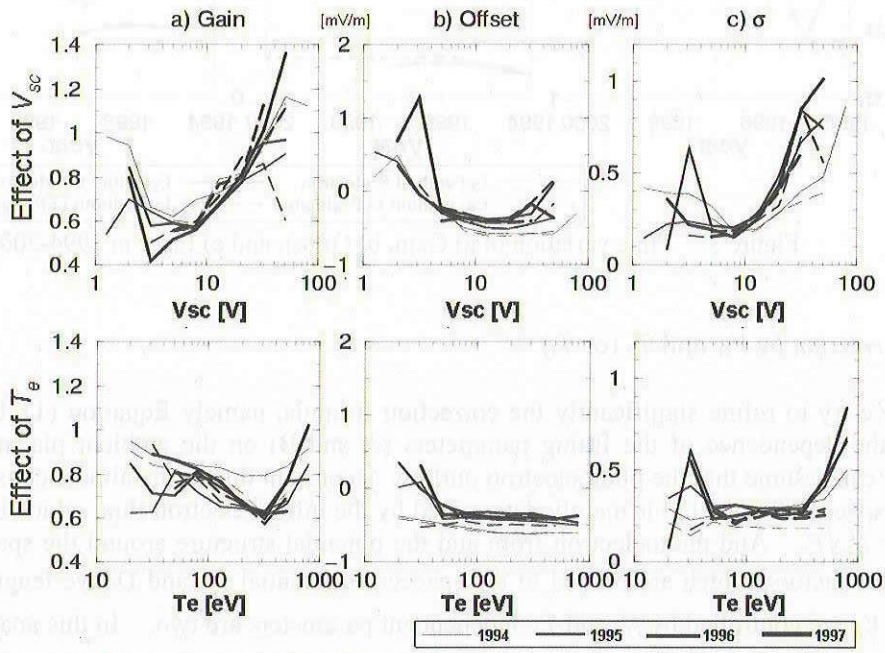

Figure 5. Dependence of a) Gain, b) Offset, and c) Error on 'V_{sc}' (Upper Dashed line is T_e = 100~158eV) and 'T_e' (Lower: Dashed line is V_{sc} = 10~15.8V.), for E_y in 1994~1997.

T_e. [EUV flux and magnetic field vector may also affect the production and motion of photoelectron. We do not take care of them in this paper.]

Figure 4 shows some samples for the relationship between $\boldsymbol{E}$ (Y-axis) and $-\boldsymbol{v}_i \times \boldsymbol{B}$ (X-axis) in 1994-1997 , selected by all criteria in Table 2, categorized by specific 'V_{sc}' and 'T_e'. Figure 5 summarizes them. Qualitatively, the effective gain is positively correlated with V_{sc}, while the offset is negatively correlated with V_{sc}. T_e has weak negative correlation with the antenna gain and offset. The correction formula for the electric field can be written by incorporating only V_{sc}, or both of V_{sc} and T_e (or T_i if T_e is unavailable) as follows:

$$(E_{real})_y = [A_0 + A_1*\log(V_{sc})] \quad (E_{obs})_y + [B_0 + B_1*\log(V_{sc})] \quad (2)$$

$$(E_{real})_y = [A_0 + A_1*\log(V_{sc}) + A_2*\log(T_e)] \quad (E_{obs})_y + [B_0 + B_1*\log(V_{sc}) + B_2*\log(T_e)] \quad (3)$$

$$(E_{real})_y = [A_0 + A_1*\log(V_{sc}) + A_2*\log(T_i)] \quad (E_{obs})_y + [B_0 + B_1*\log(V_{sc}) + B_2*\log(T_i)] \quad (4)$$

Each parameter is summarized in Table 4. We also note that T_e (and T_i) is not always reliable. Correction by Equation 2 (only by 'V_{sc}') will be easier and reliable.

E_x	A_0	A_1	A_2	B_0	B_1	B_2	σ
Correction by V_{sc}	+0.72	+0.60	--	+3.67	-1.88	--	0.49
Correction by V_{sc} & T_e	+1.19	+0.82	-0.34	+2.47	-1.99	+0.60	0.41
Correction by V_{sc} & T_i	+1.30	+0.73	-0.27	+1.92	-1.81	+0.57	0.45
E_y	A_0	A_1	A_2	B_0	B_1	B_2	σ
Correction by V_{sc}	+0.72	+0.20	--	-0.09	-0.34	--	0.33
Correction by V_{sc} & T_e	+0.99	+0.34	-0.19	+0.10	-0.37	-0.07	0.31
Correction by V_{sc} & T_i	+1.12	+0.29	-0.18	+0.04	-0.38	-0.03	0.33

Table 4. Correction by 'V_{sc}', 'V_{sc} and T_e', and 'V_{sc} and T_i' in 1995-1996 data

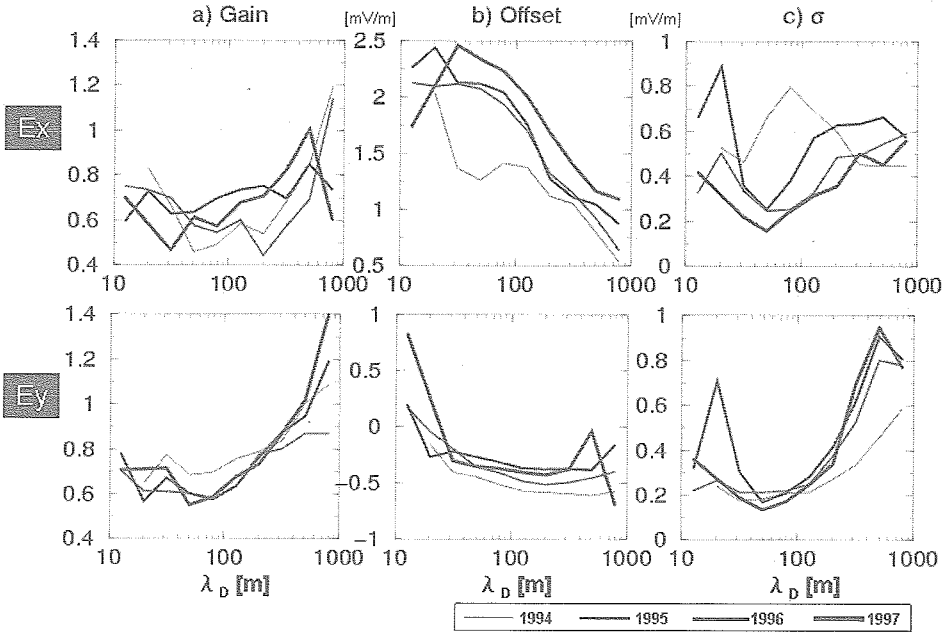

Figure 6. Dependence of a) Gain, b) Offset), and c) Error on Debye length in 1994~1997

4.3. *Effect of Spacecraft Debye Length*

We also evaluate the gain and offset in association with Debye length λ_D, which is proportional to $\sqrt{(T_e/N_e)}$. Figure 6 summarizes the result. When the Debye length is less than antenna length (102m in tip--to-tip), the gain, offset, and error of the measurement is relatively stable. On the other hand, when the antenna length beyond Debye length of ambient plasma, error becomes larger, but the electric field can still be measured. Offset in E_x is reduced, and the gain increases.

4.4. *Summary*

We conclude that the Geotail electric field measurement by the PANT system has the accuracy better than 0.5 mV/m for E_x and 0.3 mV/m for E_y. The potential accuracy of the EFD-measured electric field would be even better because those values as a result of the calibration in the present study are limited by the accuracy of the particle measurement. However, the results still includes a peculiarity that the antenna gain does not approach one as the Debye length approaches zero, and the offset does not approach zero. Since there might be errors, further refinement for the clarification will be done not only by the rejection of the ambiguity in particle observations but also by the comparison with EFD-B (electron beam technique) data [*Tsuruda et al.,* 1994].

Key of the achievement of the better accuracy of electric field measurement is 1) Reduction of the interference from the spacecraft and 2) Stability of the probe potential to the ambient plasma.

For the former requirement, the stabilization of the spacecraft potential is most important. For those purpose, the spacecraft surface materials should be conductive and grounded to the structure by low impedance, in order to keep the potential difference less than 1 V. However, the spacecraft potential itself is difficult to be reduced. It is possible by the ion beam emission from the spacecraft, but it causes disturbances to ambient plasmas. Therefore, the potential structure of the electrode is considered in order to reject the effect of 'spacecraft potential' to the probe itself. Past US and European spacecraft have been several those challenges. Most recent example is the Cluster spacecraft. Such thin space plasma condition can not be achieved in the laboratory, so the establishment of the probe design is actually difficult. Good numerical simulation is essential for such trials, and we are trying to develop and test the probe design by such methods. We will also establish the quantitative model of double probe system, including the 'shorting out' effect in the gain and the offset caused by the potential structure and non-uniform photoelectron distribution around the spacecraft [cf. *Pedersen et al.,* 1984].

For the latter requirement, the selection of the probe surface material is essential. Probe potential is determined by the photoelectron and secondary electron yields. The uniformity and the less degradation of those parameters are most important. The past spacecraft have used Aquadag, a carbon powder in the heritage of the early rocket and laboratory measurement. Recently, TiN etc. is tested [cf. Wahlstrom et al., 1992] and used as a substitute of it. The search of such material requires the cooperation between space and material scientists. Such kind of interdisciplinary cooperation will produce many contributions in all fields in future space programs.

6. Evaluation of Spacecraft Potential

Through the comparison with electron plasma frequency observed by PWI in 1992~1995, the relationship between V_{sc} (V) and N_i (/cm^3) in Geotail (Figure 7a) is approximately written as:

$$N_i = 67.1\exp\left(-\frac{V_{sc}}{1.15}\right) + 4.8\exp\left(-\frac{V_{sc}}{4.35}\right) + 0.68\exp\left(-\frac{V_{sc}}{9.15}\right) + 0.07\exp\left(-\frac{V_{sc}}{20.8}\right) \quad (5)$$

[*Ishisaka et al.*, 2001]. The Geotail EFD observation covers the wide potential range of the spacecraft potential up to 90V.

Based on the comparison with electron temperature observations, we will establish the photoelectron flux and spectrum for the planned analyses written in Section 4.4. As a preliminary model, we have already evaluated the expected spacecraft potential of BepiColombo/MMO (Mercury Magnetospheric Orbiter). For simplification, we assume the photoelectron spectrum and ambient electron temperature similar to those derived for Geotail. Result is summarized in Figure 7b. The differences between Geotail and MMO is simply caused by solar irradiance and spacecraft shape. Since the plasma density around Mercury is expected to reach less than 0.1 cm^{-3}, the spacecraft potential could rise beyond 40-50 V. Under such charge up of the spacecraft body, the spacecraft and instrument design should be optimized.

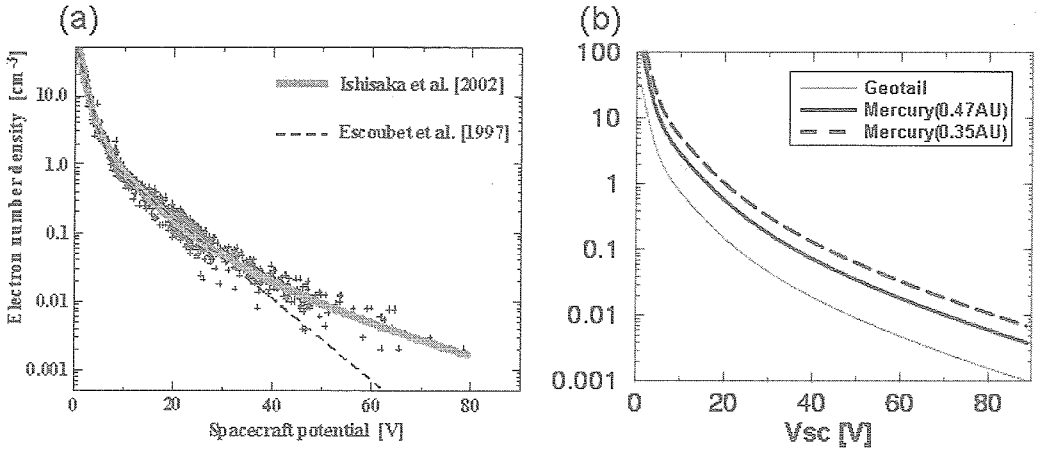

Figure 7. a) Relationship between V_{sc} (by EFD) and N_e (by PWI) in Geotail [*Ishisaka et al.*, 2001]. b) Estimation of the relationship in BepiColombo/MMO at Mercury orbit at 0.47AU (aphelion) and 0.35AU (perihelion).

References

Ishisaka, K., Okada, T., Tsuruda, K., Hayakawa, H., Mukai, T., Matsumoto, H., Relationship between the Geotail spacecraft potential and the magnetospheric electron number density including the distant tail regions, *J. Geophys. Res.*, 106, 6309-6319, 2001.

Kasaba, Y., H. Hayakawa, K. Ishisaka, T. Okada, A. Matsuoka, T. Mukai, and Y. Takei, Evaluation of DC electric field measurement by the double probe system aboard the Geotail spacecraft, Adv. Space Res., submitted, 2005.

Pedersen, A., C. A. Cattell, C.-G. F¨althammar, V. Formisano, P.-A. Lindqvist, F. Mozer, and R. Torbert, Quasistatic electric field measurements with spherical double probes on the GEOS and ISEE satellites, Space Sci. Rev., 37, 269 – 312, 1984.

Tsuruda, K., Hayakawa, H., Nakamura, M., Okada, T., Matsuoka, A., Mozer, F. S., Schmidt, R., Electric field measurements on the Geotail satellite, *J. Geomag. Geoelectr.*, 46, 693-711, 1994.

Wahlstrom et al., Thin Solid Films, 220, 315-320, 1992.